AFRL-RV-PS-
TR-2023-0010

AFRL-RV-PS-
TR-2023-0010

MODELING AND EXPERIMENT WITH 2D MATERIALS FOR CMOS TYPE DEVICES AND DIGITAL INTEGRATED CIRCUITS

Chintan P. Chavda and Georgios Veronis

Louisiana State University
202 Robert Lee Himes Hall,
Baton Rouge, LA 70803-2701

24 January 2023

Final Report

AIR FORCE RESEARCH LABORATORY
Space Vehicles Directorate
3550 Aberdeen Ave SE
AIR FORCE MATERIEL COMMAND
KIRTLAND AIR FORCE BASE, NM 87117-5776

DTIC COPY

NOTICE AND SIGNATURE PAGE

Using Government drawings, specifications, or other data included in this document for any purpose other than Government procurement does not in any way obligate the U.S. Government. The fact that the Government formulated or supplied the drawings, specifications, or other data does not license the holder or any other person or corporation; or convey any rights or permission to manufacture, use, or sell any patented invention that may relate to them.

This report is the result of contracted fundamental research which is exempt from public affairs security and policy review in accordance with AFI 61-201, paragraph 2.3.5.1. This report is available to the general public, including foreign nationals. Copies may be obtained from the Defense Technical Information Center (DTIC) (http://www.dtic.mil).

AFRL-RV-PS-TR-2023-0010 HAS BEEN REVIEWED AND IS APPROVED FOR PUBLICATION IN ACCORDANCE WITH ASSIGNED DISTRIBUTION STATEMENT.

//SIGNED//	//SIGNED//
Erin I. Vaughan Program Manager, AFRL/RVB	Mark E. Roverse, Chief AFRL Geospace Technologies Division

This report is published in the interest of scientific and technical information exchange, and its publication does not constitute the Government's approval or disapproval of its ideas or findings.

Approved for public release; distribution is unlimited.

REPORT DOCUMENTATION PAGE

Form Approved
OMB No. 0704-0188

1. REPORT DATE *(DD-MM-YYYY)*	**2. REPORT TYPE**	**3. DATES COVERED** *(From - To)*
24-01-2023	Final Report	20 Aug 2018 – 20 Aug 2022

4. TITLE AND SUBTITLE
Modeling and Experiment with 2D Materials for CMOS Type Devices and Digital Integrated Circuits

5a. CONTRACT NUMBER
FA9453-18-1-0103

5b. GRANT NUMBER

5c. PROGRAM ELEMENT NUMBER
63401F

6. AUTHOR(S)
Chintan P. Chavda and Georgios Veronis

5d. PROJECT NUMBER
2181

5e. TASK NUMBER
EF131180

5f. WORK UNIT NUMBER
V1A1

7. PERFORMING ORGANIZATION NAME(S) AND ADDRESS(ES)
Louisiana State University
202 Robert Lee Himes Hall
Baton Rouge, LA 70803-2701

8. PERFORMING ORGANIZATION REPORT NUMBER

9. SPONSORING / MONITORING AGENCY NAME(S) AND ADDRESS(ES)
Air Force Research Laboratory
Space Vehicles Directorate
3550 Aberdeen Avenue SE
Kirtland AFB, NM 87117-5776

10. SPONSOR/MONITOR'S ACRONYM(S)
AFRL/RVBN

11. SPONSOR/MONITOR'S REPORT NUMBER(S)
AFRL-RV-PS-TR-2023-0010

12. DISTRIBUTION / AVAILABILITY STATEMENT
Approved for public release; distribution is unlimited (AFRL-2023-1228 dtd 13 Mar 2023).

13. SUPPLEMENTARY NOTES

14. ABSTRACT

Two-dimensional transition metal dichalcogenides (2D-TMDs) have been proposed as novel optoelectronic materials for space applications due to their relatively light weight. MoS2 has been shown to have excellent semiconducting and photonic properties. Although ionizing gamma radiation can strongly interact with bulk materials, its effect on atomically thin materials has scarcely been investigated. Here, we report the effect of gamma irradiation on the structural and optical properties of a monolayer of MoS2. We perform Raman spectroscopy and X-ray photoelectron spectroscopy (XPS) studies of MoS2, before and after gamma ray irradiation with varying doses. The Raman spectra and XPS results demonstrate that point defects dominate after the gamma irradiation of MoS2. To understand electronic properties, we perform density functional theory (DFT) calculations.

15. SUBJECT TERMS
transition metal dichalcogenides, gamma radiation, raman spectroscopy, X-ray photoelectron spectroscopy

16. SECURITY CLASSIFICATION OF:			**17. LIMITATION OF ABSTRACT**	**18. NUMBER OF PAGES**	**19a. NAME OF RESPONSIBLE PERSON**
a. REPORT	**b. ABSTRACT**	**c. THIS PAGE**			Erin I. Vaughan
Unclassified	Unclassified	Unclassified	Unlimited	32	**19b. TELEPHONE NUMBER** *(include area code),*

This page is intentionally left blank.

TABLE OF CONTENTS

LIST OF FIGURES

Figure **Page**

ACKNOWLEDGMENTS

This material is based on research sponsored by Air Force Research Laboratory under agreement number FA9453-18-1-0103. The U.S. Government is authorized to reproduce and distribute reprints for Governmental purposes notwithstanding any copyright notation thereon.

DISCLAIMER

The views and conclusions contained herein are those of the authors and should not be interpreted as necessarily representing the official policies or endorsements, either expressed or implied, of Air Force Research Laboratory or the U.S. Government.

This page is intentionally left blank.

1. SUMMARY

Graphene is a two-dimensional material and has demonstrated an exceptional electronic and photonic properties for unlimited applications including its use in extreme environments of the space. There are several known techniques of formation of graphene onto different types of substrates such as the substrate transfer process and direct deposition. In this work, we deposited monolayer graphene over copper and nickel substrates in NanoCVD-8G Graphene reactor using argon plasma, and methane as a carbon source and studied effects of gamma irradiation using Cobalt-60 source. Radiation effects on crystalline structure of graphene is examined using Raman Spectroscopy and X-ray Photo Electron Spectroscopy (XPS). In our experiment, we used irradiation dose from 1 kGy to 2.65 kGy for different samples of graphene over copper and nickel substrates. For the graphene grown on the nickel substrates, we exposed the irradiation dose of 1.0 kGy and 2.5 kGy on two samples, respectively. For the graphene grown on the copper substrates, we exposed 1.25 kGy, 1.75 kGy, and 2.65 kGy irradiation dose on three samples, respectively. We observed D-peak in graphene deposited over nickel and copper substrates caused by disordered structure of graphene after Co-60 exposure. After the Raman spectroscopy and XPS studies, same amount of irradiation was used for second set of irradiation dose experiment. XPS data on Co-60 exposed samples showed four peaks positioned at 284.8eV, 285.3eV, 286.0 eV and 288.5 eV for C-C, C-OH, C-O-C and COOH bonds, respectively. Analysis of the results shows weakening of C-C bonds and formation of C-OH, C-O-C and COOH bonds implying reduced electrical conductivity of graphene.

Two-dimensional transition metal dichalcogenides (2D-TMDs) have been proposed as novel optoelectronic materials for space applications due to their relatively light weight. MoS2 has been shown to have excellent semiconducting and photonic properties. Although ionizing gamma radiation can strongly interact with bulk materials, its effect on atomically thin materials has scarcely been investigated. Here, we report the effect of gamma irradiation on the structural and optical properties of a monolayer of MoS2. We perform Raman spectroscopy and X-ray photoelectron spectroscopy (XPS) studies of MoS2, before and after gamma ray irradiation with varying doses. The Raman spectra and XPS results demonstrate that point defects dominate after the gamma irradiation of MoS2. To understand electronic properties, we perform density functional theory (DFT) calculations.

2. INTRODUCTION

Graphene is a two-dimensional carbon material made of carbon by covalent bonds, where carbon atoms are arranged in a honeycomb lattice [1]. Graphene has promising electronic and mechanical properties [2]. There are many processes available for the formation of the graphene. CVD (Chemical Vapor Deposition) process for the formation of graphene over the metal surface is most compatible [3]. Graphene is being investigated for its application in space electronics. In space, there are many irradiation particles and waves like x-rays, gamma rays, alpha particles, and beta particles. Single particle like neutron can create single event upset in electronic devices [4]. Graphene can work as a radiation shielding material. Graphene-metal, graphene and epsilon near zero metamaterials structure can be used for electromagnetic wave absorbent [5, 6]. Graphene/polymer, graphene/composite, graphene/epoxy composite material can work as an electromagnetic interface shielding material [7-9]. Monolayer graphene may be used for electromagnetic interface shielding [10]. Graphene and its derivatives can be used in biomedical applications like cancer imaging, and cancer targeting with appropriate surface engineering done on graphene [11]. Graphene-Schottky junctions can work as low-bias radiation sensor [12]. Since graphene is a potential material to be used in electronic devices, and radiation shielding applications, it is important to study graphene in the irradiation environment. Effects of e-beam irradiation on CVD grown graphene have been also studied [13].

In this work, we fabricated monolayer graphene over nickel and copper substrates in Moorfield nanotechnology's nanoCVD-8G reactor by CVD process. We have investigated defects and electronic behavior of irradiated graphene by the Raman spectroscopy and X-ray photo electron spectroscopy. Most of the Raman spectroscopy studies have been done after the graphene transferred on to the SiO_2/Si substrate. That process requires lift-off and other chemical processes. It can create wrinkles and defects in graphene film as well as it may increase the impurity in graphene [14].

It creates defects at the interface which has major impact on device performance. In our studies, we deposited graphene over transition metals (Ni, Cu).

Co-60 source was used for the irradiation purpose, which has nominal irradiation dose of 207 rad/Min (±5%). We have irradiated two samples of graphene grown on nickel substrate and three samples of graphene grown on copper substrate. For the graphene grown on the nickel substrate, we exposed the irradiation dose of 100 krad (1.0 kGy) and 250 krad (2.5 kGy) on sample number one and two, respectively. On graphene grown on the copper substrate, we exposed 125 krad (1.25 kGy), 175 krad (1.75 kGy), and 265 krad (2.65 kGy) irradiation on sample number one, two, and three, respectively. These irradiation doses were used for the first set of irradiations. Raman spectroscopy and X-ray photoelectron spectroscopy studies were performed on all samples (unexposed and exposed). After that, same amount of irradiation dose was subjected to samples and Raman spectroscopy and XPS studies were performed again in order to observe effect of accumulated irradiation dose.

Because of aggressive technology scaling, the channel length of silicon transistors is currently smaller than 8nm [15]. High leakage current in silicon transistors [16-18] at smaller technologies leads to sub-threshold swing of up to 60mV/decade [19]. Two-dimensional (2D) transition metal dichalcogenides (TMDs) have demonstrated promising semiconducting and optical properties [20, 21]. 2D TMD materials have good potential to lead to transistors with ultra-small channel length because of their promising applications in atomic layer devices [21-28]. MoS_2 is one of the most promising TMD materials [20, 29-31]. Graphene is one of the most widely studied 2D materials, but is challenging to use as a channel material for switching devices since it has no bandgap and a semimetal behavior [3, 32-34]. In contrast, TMD materials, such as MoS_2, $MoSe_2$, WS_2, and WSe_2, have bandgaps and show outstanding potential for future semiconductor-based devices because of their semiconducting properties [35-40]. TMD materials have also been proposed for space applications and for biomedical devices [41, 42]. In the space environment, there are many charged particles such as α and β particles, gamma rays, electrons, protons, and heavy ions. These charged particles are expected to have strong interactions with materials [43-45]. Radiation-induced defects in MoS_2, such as vacancies, interstitials, and adatoms, affect its electrical, optical, and magnetic properties [46-50]. It is therefore essential to analyze and characterize the formation of these defects in MoS_2. However, few studies have been done on irradiation effects on MoS_2 [44, 49, 51-55].

In this work, we study gamma irradiation effects on a monolayer of MoS_2. We investigate the electronic properties of irradiated MoS_2 by Raman spectroscopy and X-ray photoelectron spectroscopy (XPS). In our studies, we use a ^{60}Co source for irradiation purposes, which has a nominal irradiation dose of 191.72 rad/min (±5%). Our experimental design includes samples of single and multiple (cumulative) irradiation doses. Further, we perform density functional theory (DFT) studies to theoretically investigate the electronic properties of an irradiated monolayer of MoS_2.

3. METHODS, ASSUMPTIONS, AND PROCEDURES

3.1 Gamma Irradiation on Graphene Monolayer

In CVD process, gases are introduced in the reaction chamber and forms the intended thin film on the given substrate. By the CVD process large area of the thin film is deposited over the desired substrate. CVD is widely used technology to produce high quality graphene over large area of transition metals (Cu, Ru, Pb and Ni) substrates using hydrocarbon gases [15]. Hydrocarbon gas like methane or ethylene is introduced in the chamber which decomposes over the metallic substrate at high temperature. Metal works as a catalyst in this process. As temperature goes down, solubility of carbon atoms goes down, and carbon atoms form the intended film.

3.1.1 Chemical Vapor Deposition (CVD) Growth of Mono-layer Graphene on Transition Metal Films

Graphene Nano CVD-8G reactor from Moorfield Nanotechnology was used for the deposition of monolayer graphene over the metallic substrates of nickel and copper. In Fig. 1, schematic of cold wall resistive heater type CVD system is shown.

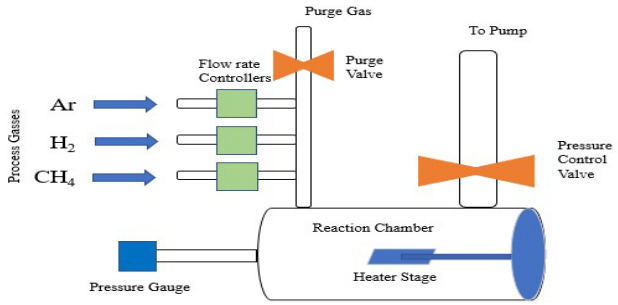

Figure 1. Schematic of gas flow in graphene nanoCVD reactor

Five different substrates of transition metals (two Ni and three Cu) were used for deposition of the monolayer graphene. Size of substrates was 1cm x 1cm. First, substrates were cleaned by isopropyl alcohol. With the carbon precursor, CH_4 = 10%, H_2 = 5%, and Ar = 85% for 120 seconds at a chamber pressure of 10 Torr at 1000°C, monolayer graphene film was deposited over the transition metal substrates.

3.1.2 Characterization of Graphene (Raman Spectroscopy)

Very important part of the graphene research is graphene's characterization. Raman spectroscopy is very widely used and well-known tool for the characterization of graphene. Raman spectroscopy is a spectroscopic method in which, light from laser source with particular wavelength, interacts with the material (in our case graphene). The light gets transmitted and scattered in the material and collected by the system of lenses. Photons from the laser source, gets absorbed in graphene. Graphene re-emits them with different and same wavelengths. Re-emitted photons are collected by the spectrometer which gives Raman spectrum. Raman scattering is an inelastic scattering of photons in the material, and there will be a change in very few numbers of photon's frequency. Most of the photon's wavelength (frequency) remains same, they may just change the direction, which is called the Rayleigh scattering.

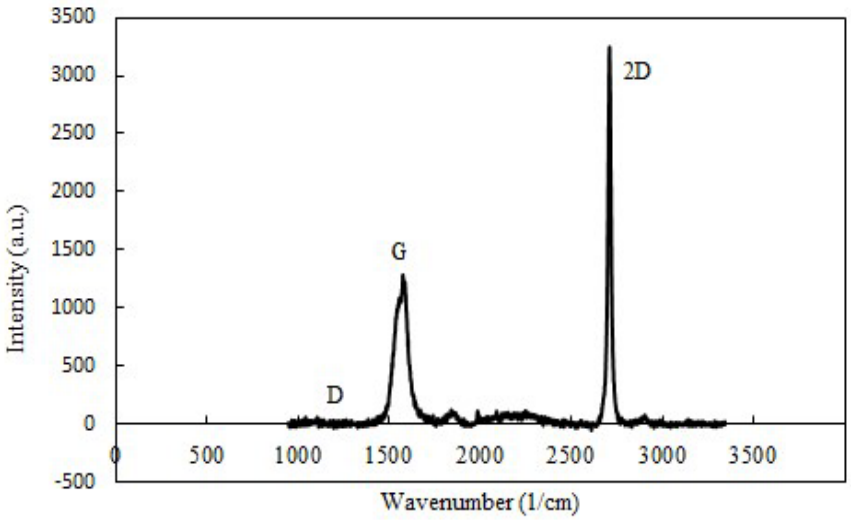

Figure 2. Raman spectrum of monolayer graphene grown over the nickel substrate

Common peaks in the Raman spectrum of graphene are D, G and 2D. In Fig. 2, Raman spectrum of monolayer CVD grown graphene over nickel substrate is shown. In Raman spectrum of graphene D peak is at 1350 cm^{-1}, G peak is at

1580 cm^{-1} and 2D peak is at 2700 cm^{-1} wavenumber. The *G* peak usually assigned to zone center phonons of *E*2*g* symmetry [16] and corresponds to the in-plane vibration of sp^2 carbon atoms. No defect is required for the activation of G peak in Raman spectrum. G peak represents the numbers of layers in the graphene. D peak is in plane, optical phonons of the crystal lattice [16] and defects are required for the activation of the D peak in Raman spectrum. D peak represents the k-point phonons of A1g symmetry of monolayer graphene. In Fig. 2, D peak, G peak and 2D peaks are shown. D peak does not exist, it means that deposited graphene over the nickel substrate has very high purity in crystalline structure.

In Raman spectroscopy results of our unexposed samples of graphene grown over nickel substrates, D peak is not being seen, which indicates that quality of graphene grown by the CVD process is very high.

3.1.3 Gamma Irradiation

For our experiment, we used Cobalt-60 (C0-60) source for the irradiation, which has nominal irradiation dose 2.07 Gy/min (207 rad/Min) (±5%). Co-60 is a radioactive isotope of cobalt. It has a half-life of 5.27 years. Co-60 can be artificially made in nuclear chamber. It is widely used source for the gamma irradiation experiment. As our Co-60 source has nominal dose rate of 2.07 Gy/min (207 rad/Min) (±5%), graphene grown on nickel sample-1 was irradiated for the 8.51 hours to achieve irradiation of 1.0 kGy, graphene grown on nickel sample-2 was irradiated for 21.25 hours to achieve 2.5 kGy and Graphene grown on copper substrate sample-1 was irradiated for 10.63 hours to achieve 1.25 kGy. Sample-2 was irradiated for 14.89 hours to achieve 1.75 kGy and sample-3 was irradiated for 22.54 hours to achieve 2.65 kGy irradiation of gamma rays. After these, Raman spectroscopy and XPS results were studied. Then for the same amount of time gamma irradiation was exposed on the same sample respectively to achieve double accumulative doses.

3.2 Gamma Irradiation on MoS_2 Monolayer

Monolayers of MoS_2 grown with chemical vapor deposition (CVD) over nickel-coated copper substrates were purchased from a 2D materials shop (6Carbon Technology). The ^{60}Co) source at the Louisiana State University Nuclear Science building was used to irradiate the materials. The source has a nominal radiation dose rate of 1.91 Gy/min (±5%). The total number of samples was $n = 4$, and samples were assigned a number # 1, 2, 3 and 4. The gamma irradiation dose was 1.92 kGy, 1.92 kGy, 2.65 kGy, and 3.0 kGy for samples # 1, 2, 3, and 4, respectively. After two weeks, samples # 1, 2, 3, and 4 were subjected to an additional dose of 1.0 kGy, 1.75 kGy, 2.65 kGy, and 3.0 kGy, respectively. After these irradiation doses, we performed Raman spectroscopy, XPS, and scanning electron microscopy (SEM) studies.

3.2.1 Gamma Irradiation Setup

Figure. 3 shows the schematic of the gamma irradiation experimental setup. We use a dry irradiator with a ^{60}Co source to irradiate the samples. Decay-corrected dose rates were calculated to determine the required irradiation time for the different samples. All samples were placed at the same position in the irradiator chamber to ensure geometrical uniformity. The samples were placed five inches from the source, based on the manufacturer's recommendations for the irradiator. The dose rate was measured to be 191.72 rad/min. The dose rate remained the same after two weeks when we performed the cumulative irradiation dose experiments.

3.2.2 Raman Spectroscopy

We used a Renishaw inVia Reflex Raman spectroscope for the Raman experiments. We used a laser excitation wavelength of 532 nm in all experiments. The objective lens used was 50x, and the acquisition time was 10 seconds. We used the extended mode. The spectra were analysed using WiRE 5.3. We analysed its peaks using the OriginPro software suite.

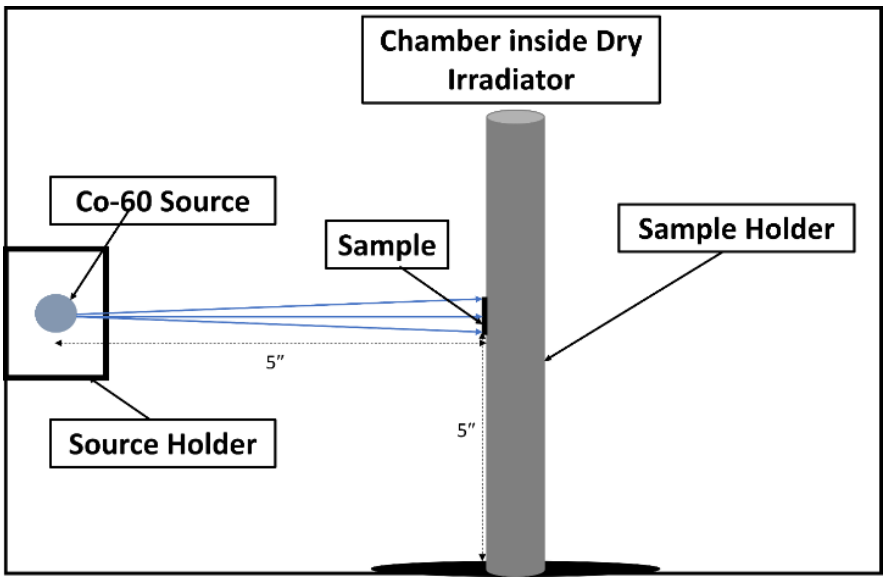

Figure 3. Gamma irradiation experimental setup using ^{60}Co source inside irradiator

3.2.3 X-ray Photoelectron Spectroscopy

We used a Scienta Omicron ESCA 2SR X-ray Photoelectron spectroscope for our XPS observations. It is equipped with a Mg/Al monochromatic source. The CASA XPS software package was used for the analysis of the XPS data.

3.2.4 DFT Calculations

DFT computational studies were performed using the Quantum Espresso Suite [56, 57]. We perform DFT studies to investigate the electronic properties of pristine and irradiated monolayers of MoS_2.

4. RESULTS AND DISCUSSION

4.1 Raman Spectroscopy Studies for Graphene

4.1.1 Monolayer Graphene Grown on Nickel Substrate

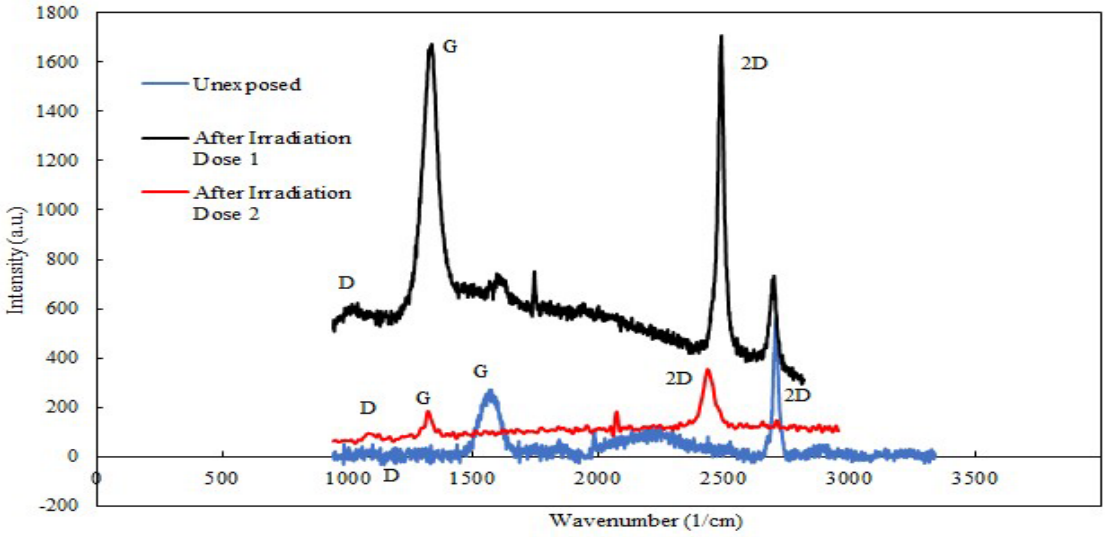

Figure 4. Raman spectra of CVD graphene grown on nickel substrate, with and without irradiation doses for sample-1

Monolayer graphene grown over nickel substrate was subjected to 100 krad (1.0 kGy) first and again it was subjected to same amount of dose. For the second dose, the accumulative dose was 200 krad (2.0 kGy). In Fig. 4, Raman spectrum of monolayer graphene grown over the nickel substrate is shown. Three different curves represent different irradiation doses. In blue curve (unexposed graphene grown over nickel substrate), there is no D peak, because of purity in crystalline structure of graphene. D peak is clearly shown after 100 krad (1.0 kGy) of irradiation on sample-1, which indicates that the defects are created on the monolayer graphene after the 100 krad (1.0 kGy) of irradiation.

On the sample-2 which was subjected to a dose of 250 krd (2.5 kGy), has a bigger D-peak than sample-1's D peak. It suggests that because of the higher irradiation dose the more defects are created on sample-2 after first set of irradiation doses. Raman spectrum of sample-2 graphene grown over the nickel substrate is shown in Fig. 5.

Furthermore, analysis of Raman spectra of non-irradiated and irradiated graphene grown over the nickel substrate shows that after the 100 krad (1.0 kGy) of irradiation of gamma rays, red shift in G and 2D peak is shown. After increasing the irradiation doses blue shift is being seen on G and 2D peak of the Raman spectra of irradiated graphene over the nickel substrate. The red shift occurred because of the strain induced phonon softening by the symmetry breaking in the crystalline structure of the monolayer graphene [17]. In our case, phonon softening introduced by the defects created after the gamma irradiation. The blue shift occurred after further irradiation, which is attributed to the doping in graphene by the charge from the metallic substrate. The same effect has occurred in monolayer graphene grown over the SiO_2/Si, by the charge impurity from substrate [18].

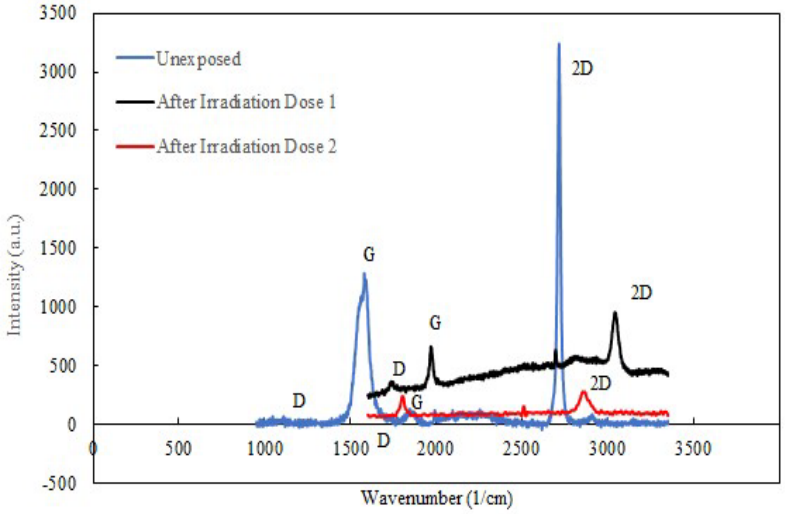

Figure 5. Raman spectra of CVD graphene grown on nickel substrate, with and without irradiation doses for sample-2

4.1.2 Monolayer Graphene Grown on Copper Substrate

For the graphene grown on copper substrates, three samples were used for the irradiation. Samples were subjected to irradiation doses of 125 krad (1.25 kGy), 175 krad (1.75 kGy), and 265 krad (2.65 kGy), respectively for the samples1, 2 and 3, respectively for the first set of irradiations. D-peak was created and/or D peak became bigger or wider in all samples. After the initial set of irradiation red shift is being seen and then blue shift is being seen on G and 2D peaks in Raman spectra of all the samples of graphene grown over the copper. The red shift in G peak and 2D peak is due to the strain-induced phonon softening by creating defects by the gamma irradiation in mono layer graphene [2].

Raman spectrum of samples1, 2 and 3 is shown in the Fig. 6, 7 and 8, respectively. In sample-1, no D peak was observed for the unexposed sample and after the exposer of gamma rays D peak is clearly seen, which is the indication that defects are created in monolayer graphene after irradiation of gamma rays. In all samples Raman shift is clearly shown. There is a significant change in full width half maximum of G and 2D peaks in all samples, which suggests defects are disordered in all samples [2].

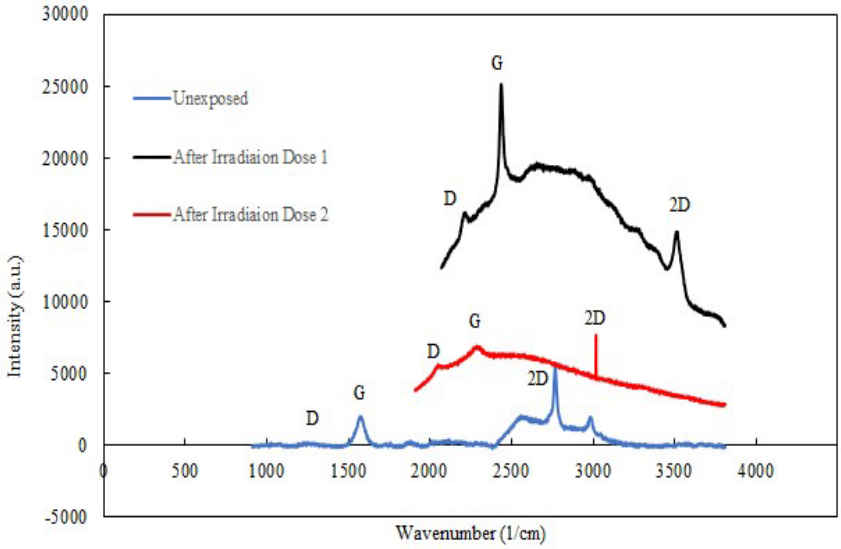

Figure 6. Raman spectra of CVD graphene grown on copper substrate, with and without irradiation doses for sample-1

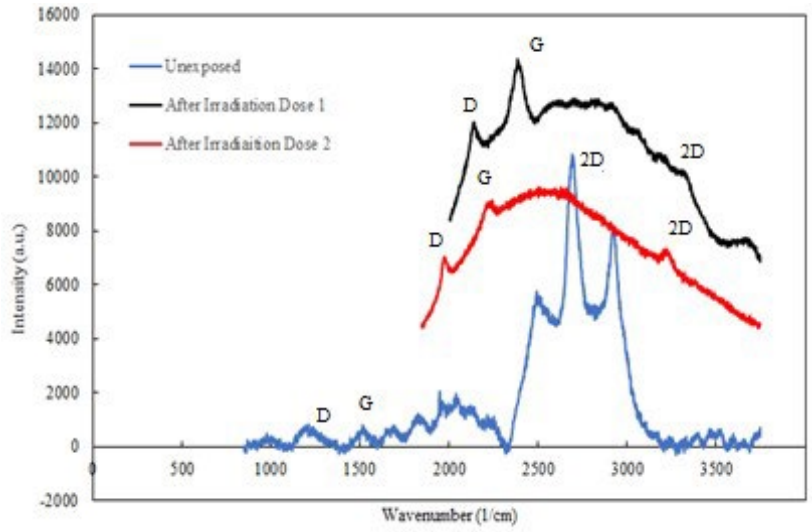

Figure 7. Raman spectra of CVD graphene grown on copper substrate, with and without irradiation doses for sample-2

For further investigation, we plotted intensity of D peak versus intensity of G peak (I_D/I_G) curve. In Fig. 9 and 10, I_D/I_G curve for graphene grown over nickel substrate and graphene grown over copper substrate is shown. Initially, I_D increases with respect to I_G, after some irradiation doses, the I_D started to decrease with respect to I_G for both kinds of samples (graphene grown over the nickel substrate and graphene grown over the copper substrate). With the increase in irradiation dose, D peaks show up and widen, respectively. But as irradiation doses are increasing the crystalline structure has changed to amorphous. In amorphous carbon structures, development of a D peak indicates ordering exactly opposite of the graphene (crystalline structure). Because of the reordering of amorphous carbon structure, the I_D versus I_G curve comes down. The first trend increase in I_D/I_G indicates the crystalline graphene changed into nanocrystalline graphene, and the second trend, decrease in I_D/I_G, is due to the transformation of nanocrystalline graphene to mainly sp2 amorphous carbon film [16].

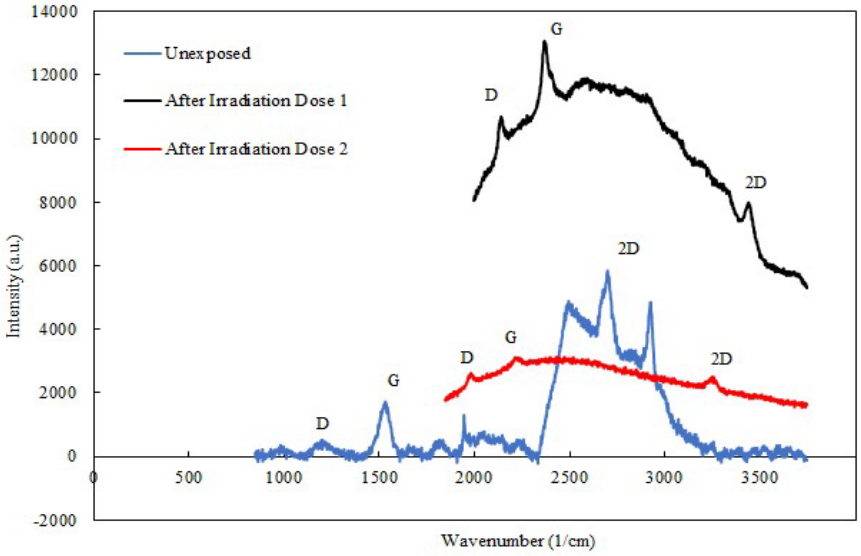

Figure 8. Raman spectra of CVD graphene grown on copper substrate, with and without irradiation doses for sample-3

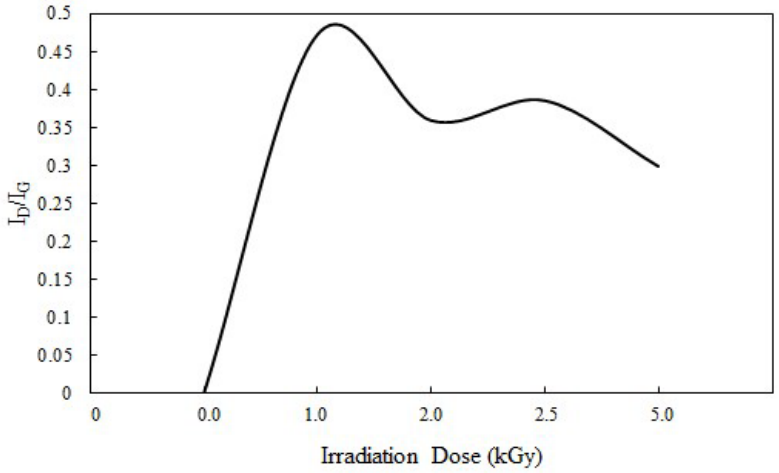

Figure 9. Evolution of I_D/I_G curve as a function of irradiation dose for graphene grown over nickel substrate

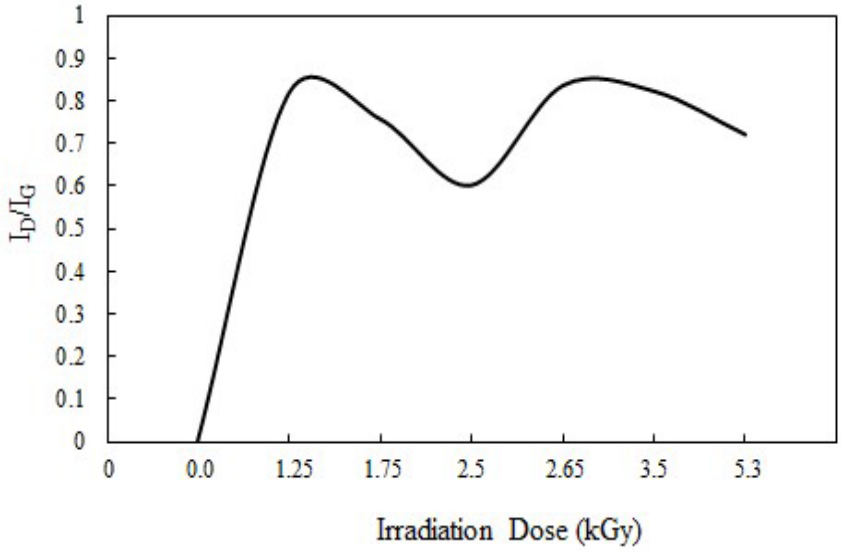

Figure 10. Evolution of I_D/I_G curve as a function of irradiation dose for graphene grown over copper substrate

4.2 X-Ray Photoelectron Spectroscopy (XPS) Studies for Graphene

XPS study is very important in our case, because we want to study the conductivity of graphene in radiation harsh environment. XPS studies show the possible doping in graphene. XPS is a surface sensitive measurement technique. Sample is subjected to x-rays and with its energy, electrons excite into vacuum. Then electrons are collected by the collectors. Information of numbers of electrons and kinetic energy of electron are used to interpret the valuable information. We used Scienta Omicron ESCA 2SR XPS for our studies. It is equipped with Mg/Al monochromatic source. CASAXPS software package was used for the analysis of the XPS data. We plotted different curves for C-C, C-OH, C-O-C and -COOH bonds. The XPS data is represented with 4 peaks, which are positioned at 284.8 eV, 285.3 eV, 286.0 eV, and 288.5 eV for C-C, C-OH, C-O-C, and -COOH bonds, respectively. In Fig. 11, XPS data of CVD graphene grown over the nickel substrate is shown.

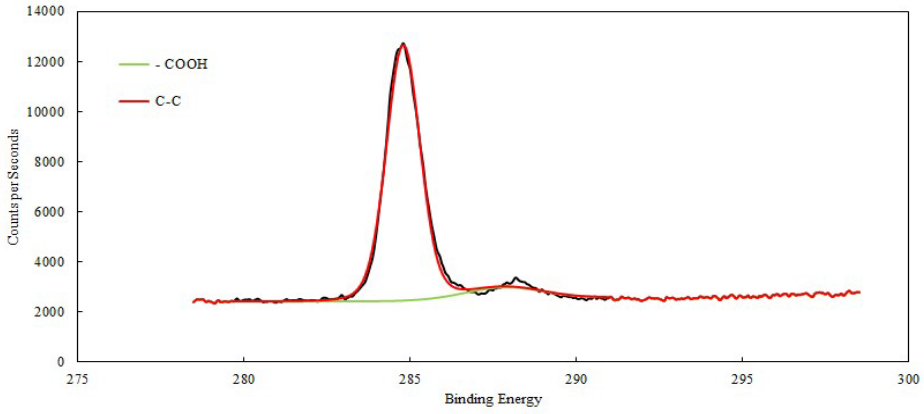

Figure 11. XPS studies of CVD graphene grown on nickel substrate (unexposed)

The sample is unexposed to any irradiation. C-C bond-area is very high (89.59%). In Table 1 and Table 2, percent bond area covered by each peak of total C1s for all samples after each irradiation dose is shown. From Table 1 and Table 2, it is seen that, as the irradiation dose increases the C-C bond area decreases and C-OH, C-O-C, and COOH peak area increases. It indicates that, by the irradiation, C-C bond has broken up and carbon atoms of the graphene

made different bonds like C-OH, C-O-C and, COOH, which means that the electrical conductivity of graphene has reduced by the gamma irradiation. Gamma irradiation increases the adsorption of oxygen atoms in graphene.

Table 1. XPS data- bond area interpretation for CVD graphene grown over nickel sample

Bonds	Gr/Ni Samples				
	Unexposed (Bond Area %)	Sample 1 (Bond Area %)		Sample 2 (Bond Area %)	
		1.0 kGy	2.0 kGy (Accumu-lative)	2.5 kGy	5.0 kGy (Accumu-lative)
C-C	89.54	84.43	69.85	61.88	38.97
C-OH	-	-	25.68	24.30	43.13
C-O-C	-	-	-	13.81	18.19
-COOH	10.46	15.57	8.47	-	-

Table 2. XPS data- bond area interpretation for CVD graphene grown over copper sample

Bonds	Gr/Cu Samples						
	Unexposed (Bond Area %)	Sample 1 (Bond Area %)		Sample 2 (Bond Area %)		Sample 3 (Bond Area %)	
		1.25 kGy	2.5 kGy (Accumu- lative)	1.75 kGy	3.5 kGy (Accumu-lative)	2.65 kGy	5.3 kGy (Accumu-lative)
C-C	52.48	31.06	24.80	27.99	30.82	34.84	28.76
C-OH	35.92	37.66	69.60	60.93	52.17	58.38	42.81
C-O-C	-	25.07	-	5.41	9.70	4.02	15.68
-COOH	11.60	6.21	5.60	5.67	7.31	8.84	6.67

4.3 Raman Spectroscopy Studies for MoS_2

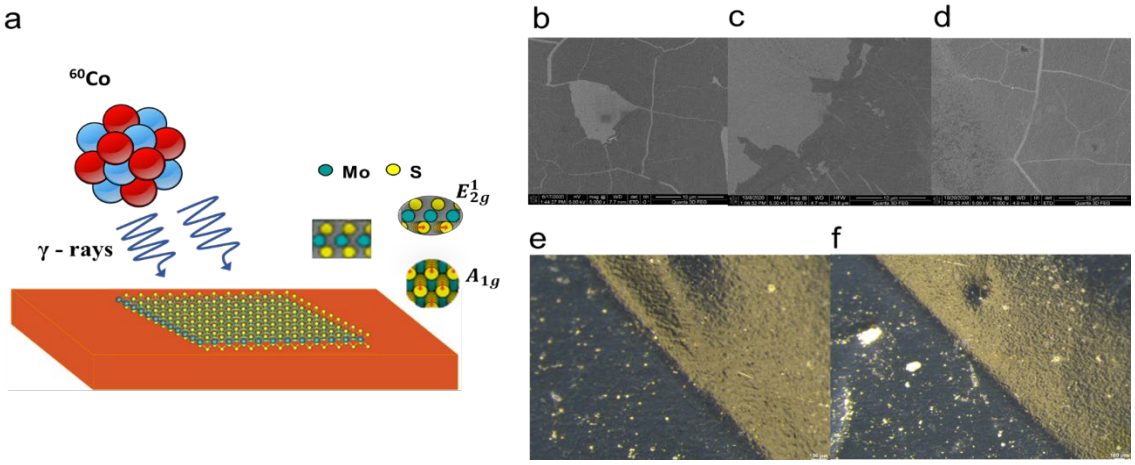

Figure 12. (a) Gamma irradiation on monolayer MoS_2 over copper substrate. (b) SEM image of pristine MoS_2. (c) SEM image of irradiated MoS_2 with 1.92 kGy. (d) SEM image of irradiated MoS_2 with cumulative dose of 5.30 kGy. (e) Optical image of pristine MoS_2. (f) Optical image of irradiated MoS_2 with cumulative dose of 6.0 kGy

Figure 12(a) schematically shows the interactions of gamma rays with MoS_2. Gamma ray irradiation plays an important role and contributes to pair production, Compton scattering, point defects of atoms (vacancies), and fast electrons [58]. All of these may lead to changes in the structural and electronic properties of monolayer MoS_2.

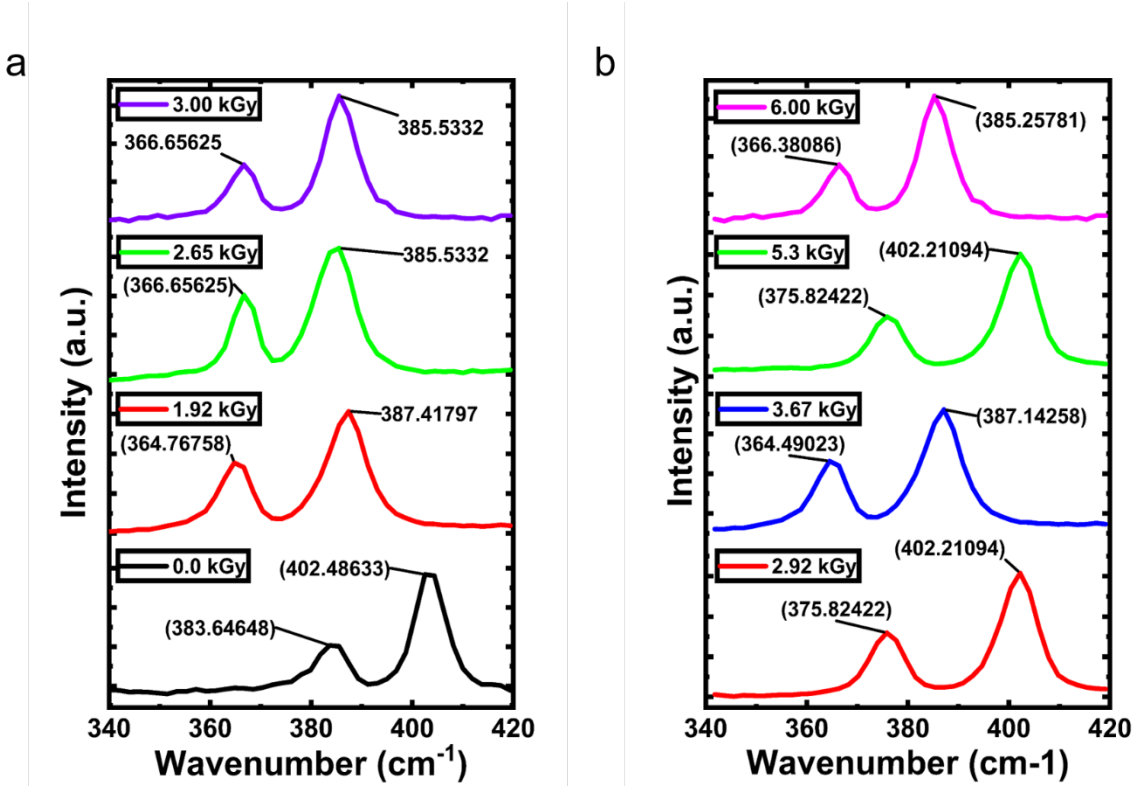

Figure 13. (a) Raman spectra results of monolayer MoS_2 after the first set of irradiation doses. (b) Raman spectra results of monolayer MoS_2 after the second set of irradiation doses (cumulative doses)

Common peaks in the Raman spectra of a monolayer of MoS_2 are E^1_{2g} (384.7 cm^{-1}), and A_{1g} (403.6 cm^{-1}) at the Γ point in the Brillouin zone of a hexagon of monolayer MoS_2, according to group theory [59] (the schematic of the vibrations is shown in the inset of Fig. 12(a)) . The E^1_{2g} mode is the result of the vibrations of two sulphur atoms with respect to the molybdenum atom, while the A_{1g} mode corresponds to the out-of-plane vibration of sulphur atoms in the opposite direction [59]. The SEM images of the MoS_2 sample before (Fig. 12(b)) and after (Figs. 12(c) and 12(d)) gamma-ray irradiation did not show appreciable changes. The corresponding optical images are shown in Figs. 12(e) (before irradiation) and 12(f) (after irradiation).

To describe the structural changes, we studied the Raman spectra of irradiated MoS_2. The Raman spectra quantitatively describe the changes in the structural properties of monolayer MoS_2. As mentioned in the Materials and Methods section, we use four samples of monolayer MoS_2 grown over a nickel-coated copper substrate. Figures 13(a) and 13(b) show the Raman spectra after the first and second cumulative irradiation doses, respectively. At the excitation resonance condition of λ = 532 nm, we observed two prominent peaks at 384.7 cm^{-1} and 403.6 cm^{-1} (Fig. 13(a)) corresponding to the E^1_{2g} and A_{1g} vibrational modes, respectively [59]. We shift the Raman spectra corresponding to different irradiation doses vertically for clarity. We show the E^1_{2g} peak Raman shift as a function of irradiation dose in Fig. 13(a). We observe that after an irradiation dose of 1.92 kGy both the E^1_{2g} and A_{1g} intensity peaks red- shift to a lower Raman frequency (Fig. 13(a)). For single doses of 2.65 kGy and 3.0 kGy of irradiation, blue shift of the Raman frequency occurs compared to the Raman frequency at 1.92 kGy (although these Raman frequencies are still red-shifted compared to the pristine MoS_2 sample) (Fig. 13(a)). Fig. 13(b) shows the effect of cumulative doses on the Raman spectra. The cumulative doses show a zig-zag pattern with Raman frequencies jumping from a red shift to a blue shift repetition pattern with the increase of doses. After 3.67 kGy of gamma ray irradiation a redshift appears on the E^1_{2g} and A_{1g} intensity peaks compared to 2.92 kGy. With further irradiations, blueshift and redshift appear after 5.30 kGy and 6.00 kGy, respectively (Fig. 13(b)). Using DFT calculations, it was shown that S defects lead to redshift

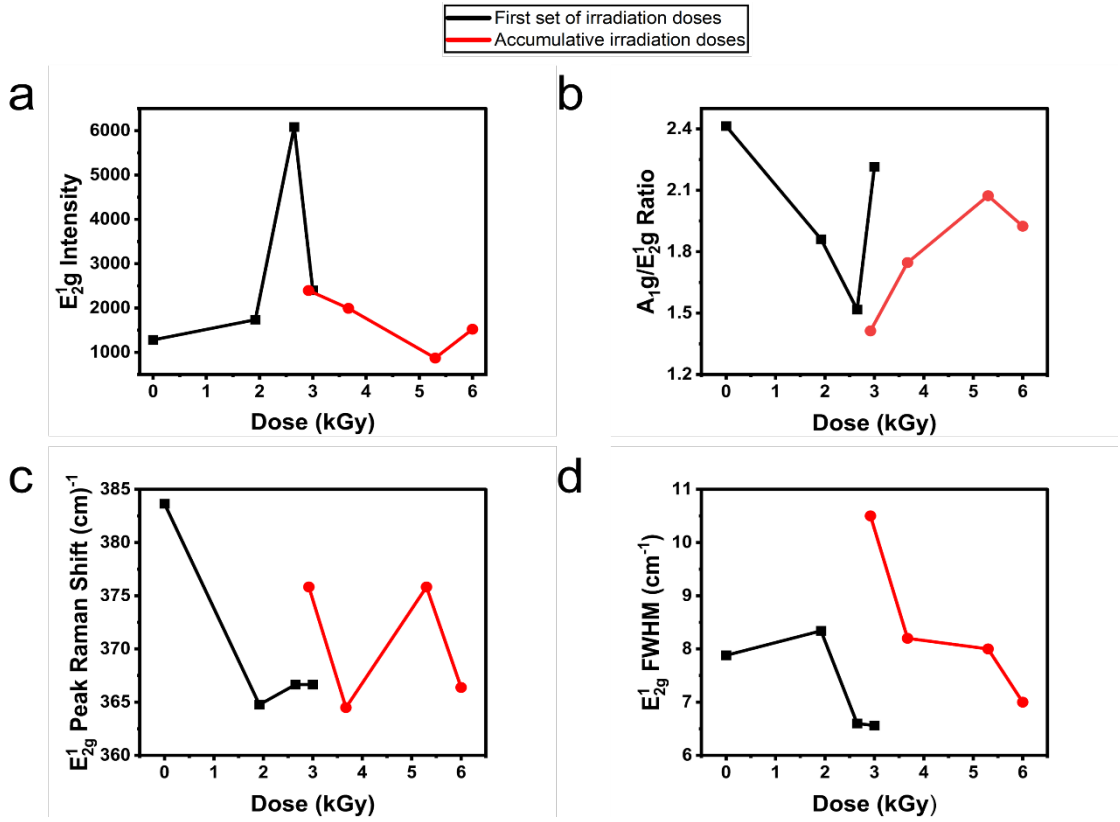

Figure 14. (a) E^1_{2g} peak intensity as a function of irradiation dose. (b) A_{1g}/E^1_{2g} peak intensity ratio as a function of irradiation dose. (c) E^1_{2g} peak Raman shift as a function of irradiation dose. (d) E^1_{2g} peak full width half maximum (FWHM) as a function of irradiation dose

in the E^1_{2g} and A_{1g} peaks. Mo defects lead to blueshift in the E^1_{2g} and A_{1g} peaks of the Raman spectra of monolayer and bulk MoS_2 [60]. Based on our results, we hypothesize that after the first irradiation dose, S defects dominate in both cases (first set of irradiation dose of 1.92 kGy and initial cumulative irradiation dose of 2.92 kGy). The reasoning is that, since the S atom is lighter than the Mo atom, it will be evicted first [61]. As we increase the irradiation doses, we observe both kinds of shift (redshift and blueshift) in cumulative irradiation doses observation (Figs. 13(a) and 2.3(b)). This points to the possible formation of S and Mo point defects in the structure of monolayer MoS_2.

Figure 14(a) shows the E^1_{2g} peak intensity as a function of irradiation dose. The black curve is for single dose experiments, and the red curve is for cumulative dose experiments. The E^1_{2g} peak intensity increases up to 2.65 kGy, and then decreases when the single dose is increased to 3.0 kGy. Higher doses of radiation decrease the E^1_{2g} peak intensity (for single dose and accumulative dose), which could be due to the formation of more defects leading to extra strain in the atomic structure of monolayer of MoS_2. Literature data show that the extra strain is generally responsible for the degradation of the E^1_{2g} peak [62].

In Fig. 14(b) we show the intensity ratio of the A_{1g} and E^1_{2g} peaks as a function of irradiation dose. Initially, with 1.92 kGy of irradiation dose, A_{1g}/ E^1_{2g} decreases. This is the result of missing S atoms [63]. Missing S atoms result in the relative decrease of the A_{1g} mode [60], [63-65]. As we increase the irradiation dose, after 3.0 kGy of irradiation dose, the A_{1g}/ E^1_{2g} intensity increases, which may be due to the appearance of Mo vacancies after a higher amount of gamma irradiation [66]. The A_{1g}/E^1_{2g} intensity ratio feature in the Raman spectra of irradiated MoS_2 samples shows that at low irradiation doses the S defects dominate [61]. Figure 14(c) shows the E^1_{2g} Raman shift as a function of irradiation dose. Shift to lower frequencies (red shift) in Raman peaks, and especially in the E^1_{2g} peak, indicates large cluster removal, such as MoS_4 or MoS_6 [62]. The intensity ratio A_{1g}/ E^1_{2g} and the E^1_{2g} Raman shift, as shown in Figs. 14(b) and 3(c), respectively, taken together suggest the formation of point defects by the gamma radiation [67]. Unlike the results previously shown in the literature [60, 62], we did not find defect-induced Raman peaks at the lower frequency side of the E^1_{2g} peak. In Fig. 14(d) we show the full width at half maximum (FWHM) of the E^1_{2g} peak as a function of irradiation dose. We observe that the FWHM of the E^1_{2g} peak decreases with the increase of radiation doses. The mechanical stress and strain in the structure are responsible for the degradation in the FWHM of the E^1_{2g} peak [62, 65]. Literature data [62, 65, 67] also suggest that the linewidth of the E^1_{2g} peak decreases with the increment of point defects by ion radiation and mechanical strain.

4.4 XPS Studies for MoS_2

We perform XPS studies to further analyse the gamma irradiation effects on a monolayer of MoS_2 (Fig. 15). In the survey spectra of pristine MoS_2 XPS study, we found peaks for nickel, oxygen, and carbon. Our samples are CVD-grown MoS_2 over nickel coated copper; hence Ni and Cu peaks appear in the survey spectra. The carbon peak is due to the presence of hydrocarbon in the XPS instrument itself and was utilized to calibrate the system. The peaks at 229.1 eV and 232.3 eV observed in the XPS spectra of pristine molybdenum are identified as Mo $3d_{5/2}$ and Mo $3d_{3/2}$, respectively, and the small shoulder around 226 eV in Fig. 15(a) is the sulphur 2s peak. In the pristine MoS_2 spectra of XPS, S consists of S $2p_{3/2}$ and S $2p_{1/2}$ peaks at 162 eV and 163.2 eV, respectively (Fig. 15(e)) [68]. The evolution of Mo and S peaks at different doses are shown in Figs. 15(b)-2.5(d), and Figs. 15(f)-15(h), respectively.

We show different atoms peak area of XPS spectra as a function of irradiation dose in Fig. 16(a). We observe that with the gamma irradiation, the XPS peak area for both atom types (Mo and S) is decreasing after an initial dose of 1.92 kGy irradiation, and remains almost constant with higher irradiation doses of 2.65 kGy. For cumulative double doses, the area of both atom types is decreasing for irradiation doses from 2.92 kGy to 3.67 kGy. Figures 16(b) and 2.6(c) show the changes in Mo and S XPS peak positions as a function of irradiation dose. The Mo 3d peak positions do not show appreciable changes after irradiation doses (Fig. 16(b)). The S $2p_{3/2}$ peak shows blue shift to higher binding energy after 1.92 kGy of irradiation compared to the no radiation case; however, for the cumulative doses of gamma radiation samples, we observe red shift of the XPS peaks to lower binding energy on the S $2p_{3/2}$ peak for all samples (Fig. 16(c)). The S $2p_{1/2}$ peak shows similar trend with the irradiation doses. These results suggest that in the case of MoS_2 monolayer sample, as we increase the irradiation dose, first S and later Mo defects appear [69]. In Fig.

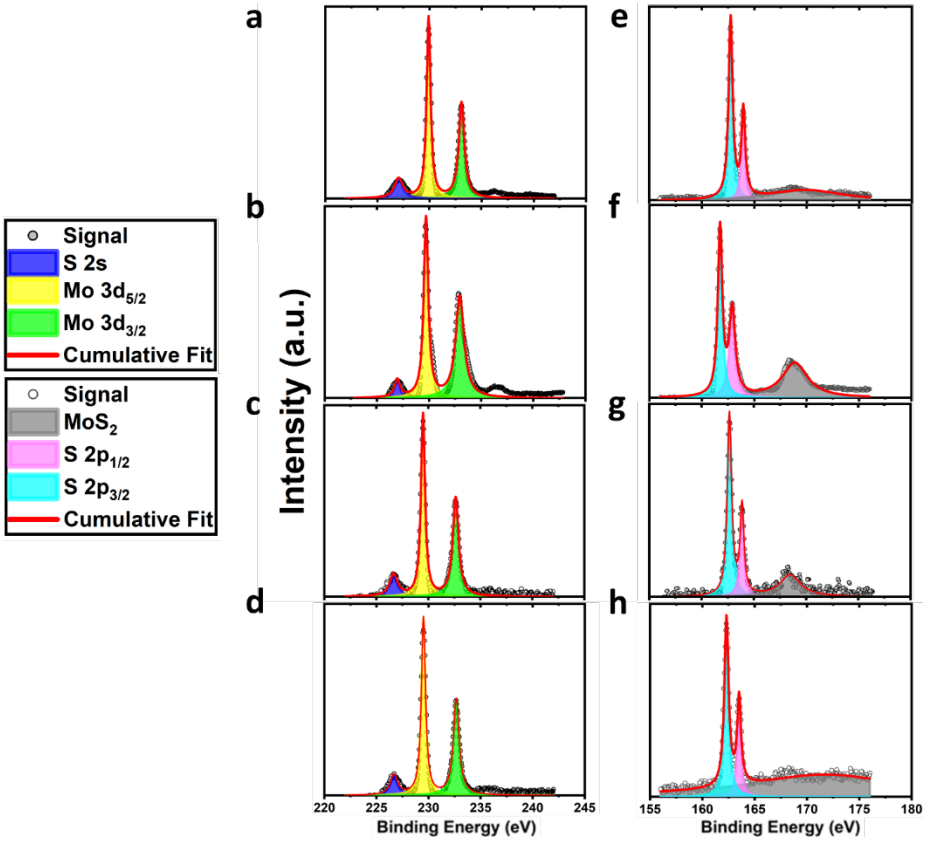

Figure 15. XPS spectra of MoS_2. Mo d components with (a) 0 kGy; (b) 1.0 kGy; (c) 1.75 kGy; (d) 2.65 kGy of irradiation. S 2p components with (e) 0 kGy; (f) 1.00 kGy; (g) 1.75 kGy; (h) 2.65 kGy of irradiation

16(d), we show the FWHM for different peaks of the MoS_2 XPS spectra as a function of irradiation dose. By the first 1.92 kGy of irradiation, the FWHM of S $2p_{3/2}$ and Mo $3d_{3/2}$ increases. The FWHM trend of S $2p_{3/2}$ and Mo $3d_{3/2}$ suggests that the quality of MoS_2 is degraded because of gamma irradiation [70]. Further, we show the area ratio of Mo to S peak as a function of irradiation dose in Fig. 16(e). For the first set of irradiations, the molar area ratio of Mo/S decreases and after higher irradiation doses it increases. This trend suggests that initially S defects are formed by a small amount of irradiation, and, after increasing the irradiation dose, Mo defects are also appearing. After even higher irradiation doses, S defects are more in quantity. The same trends are observed in the cumulative dose studies (Fig. 16(b), red curve). S defects are more likely to be dominant because S atoms are lighter than Mo atoms [71]. From the areas of the Mo $3d_{3/2}$ and S $2p_{3/2}$ peaks, we calculate the Mo:S atomic ratio R_{Mo-S} as

$$R_{Mo/S} = (A_{Mo}/F_{Mo})/(A_s/F_s), \qquad \ldots(1)$$

where A_{Mo} and A_S are the peak areas of the Mo $3d_{3/2}$ and S $2p_{3/2}$ peaks, respectively; F_{Mo} and F_S are relative sensitivity factors (RSFs) of the Mo 3d3/2 and S 2p3/2 peaks, respectively. RSFs are calculated by the CasaXPS software. After the highest amount of irradiation in both cases (single dose and cumulative dose), we believe that MoS_2 becomes amorphous [70]. We observe that, as the irradiation dose increases, the Mo $3d_{5/2}$, S $2p_{1/2}$, and S $2p_{3/2}$ peaks are moving towards higher binding energies on the XPS spectra. The S 2p peaks increase by 6% in intensity compared to the ones in the pristine sample (Fig. 16(a)). Our XPS study suggests that sulphur defects appear first in the MoS_2 structure at lower irradiation dose level, followed by Mo defects at higher irradiation.

4.5 Electronic Property Study for MoS_2

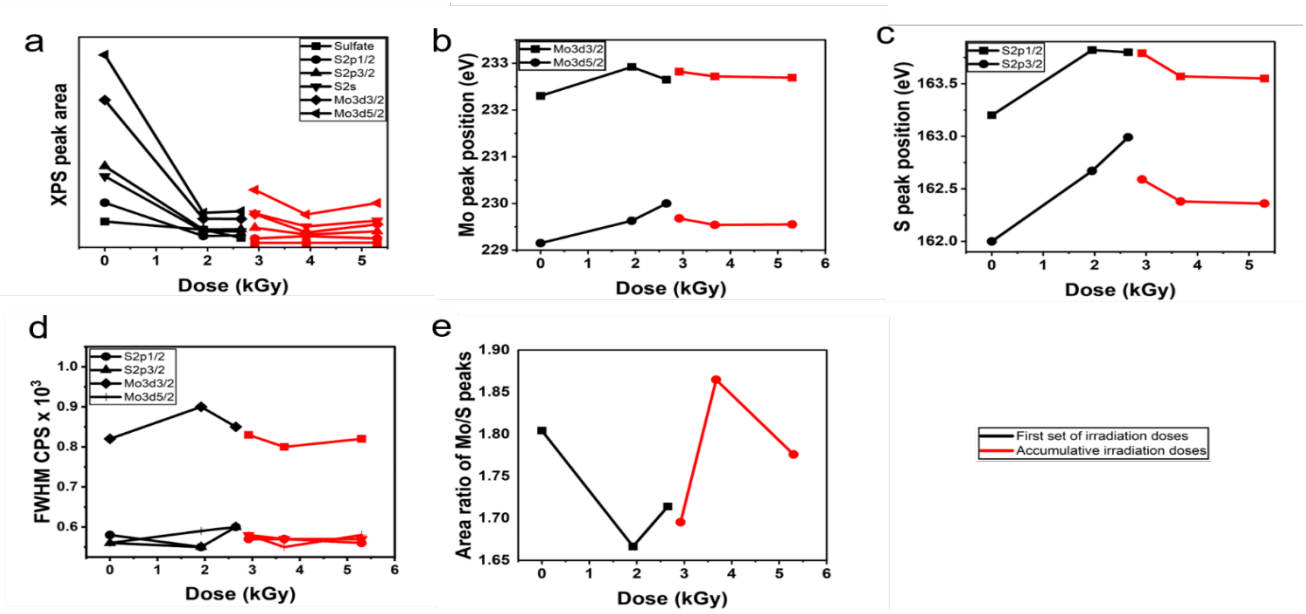

Figure 16. (a) XPS peak area as a function of irradiation dose after the first and second set of irradiation doses. (b) XPS peak position of Mo as a function of irradiation dose. (c) XPS peak position of S as a function of irradiation dose. (d) Full width at half maximum (FWHM) of XPS peaks as a function of irradiation dose. (e) Area ratio of Mo and S peaks as a function of irradiation dose

Our Raman spectra and XPS studies, as well as literature data in Refs. [60, 61, 65], suggest that point defects are the main defects in the MoS_2 structure after receiving irradiation doses. We examine the electronic properties of irradiated MoS_2 using DFT. More specifically, we perform DFT studies using the Quantum Espresso suite to obtain the electronic properties of pristine and irradiated (with defect) MoS_2. We perform our studies on a 5x5 supercell of monolayer MoS_2. The Quantum Espresso suite solves the Kohn-Sham equation to obtain the electronic properties of a system. The solution of the Kohn-Sham equation allows the Quantum Espresso suite to determine the band structure, density of states, and the charge density. In Fig. 17(a) we show the atomic structure of pristine MoS_2, its band structure, and density of states. We found that the pristine MoS_2 has a bandgap of 1.83 eV, which agrees with the literature reported value [72]. With the formation of defects, the bandgap decreases (Table 3). Figure 17(a) (middle figure) shows the band structure diagram of monolayer MoS_2 with high symmetric points in the first Brillouin zone shown in the x-axis and the corresponding energy values in the y-axis. Since our experimental results suggested that at lower radiation doses S and Mo defects appear, we performed DFT simulations on the structure of MoS_2 by removing 1S, 2S, and 1 Mo & 2S atoms in the supercell (Figs. 17(b)-17(d)). The 1S (Fig. 17(b)), and 2S (Fig. 17(c)) defects open narrow bandgaps of 1.03 eV and 0.98 eV, respectively. The bandgap value decreases with increase of defect concentration. This may lead to better conductivity in 2S defected MoS_2 compared to MoS_2 with 1S defect. With the formation of defects, the bands split and cross the Fermi energy level, as shown in the band diagrams. The Fermi energy of the defected MoS_2 is different from the one of pristine MoS_2 (Table 3). This is due to the movement of charge carriers in the structures as a result of the formation of defects. We also show the corresponding total density of states (DOS) for each system (Figs. 17(a)-17(d), right). The DOS at Fermi energy (E = 0) for the pristine MoS_2 is zero, while for the defected MoS_2 the DOS is found to be non-zero. The simulations improve our understanding of the changes in the electronic structure of MoS_2 due to the creation of S and Mo vacancies.

Table 3. Electronic properties of pristine and defected MoS_2

Data of band structures, DOS (eV)	MoS_2	1S defect in MoS_2	2S defect in MoS_2	1Mo 2S defect in MoS_2
E_f (Fermi Energy)	3.1637	2.8485	2.7394	2.4336
E_g(Bandgap Energy)	1.83	1.0257	0.9759	0.8687
E_t(Total Energy)	-4516.31683242	-4495.54378458	-4474.87910457	-4335.08260142

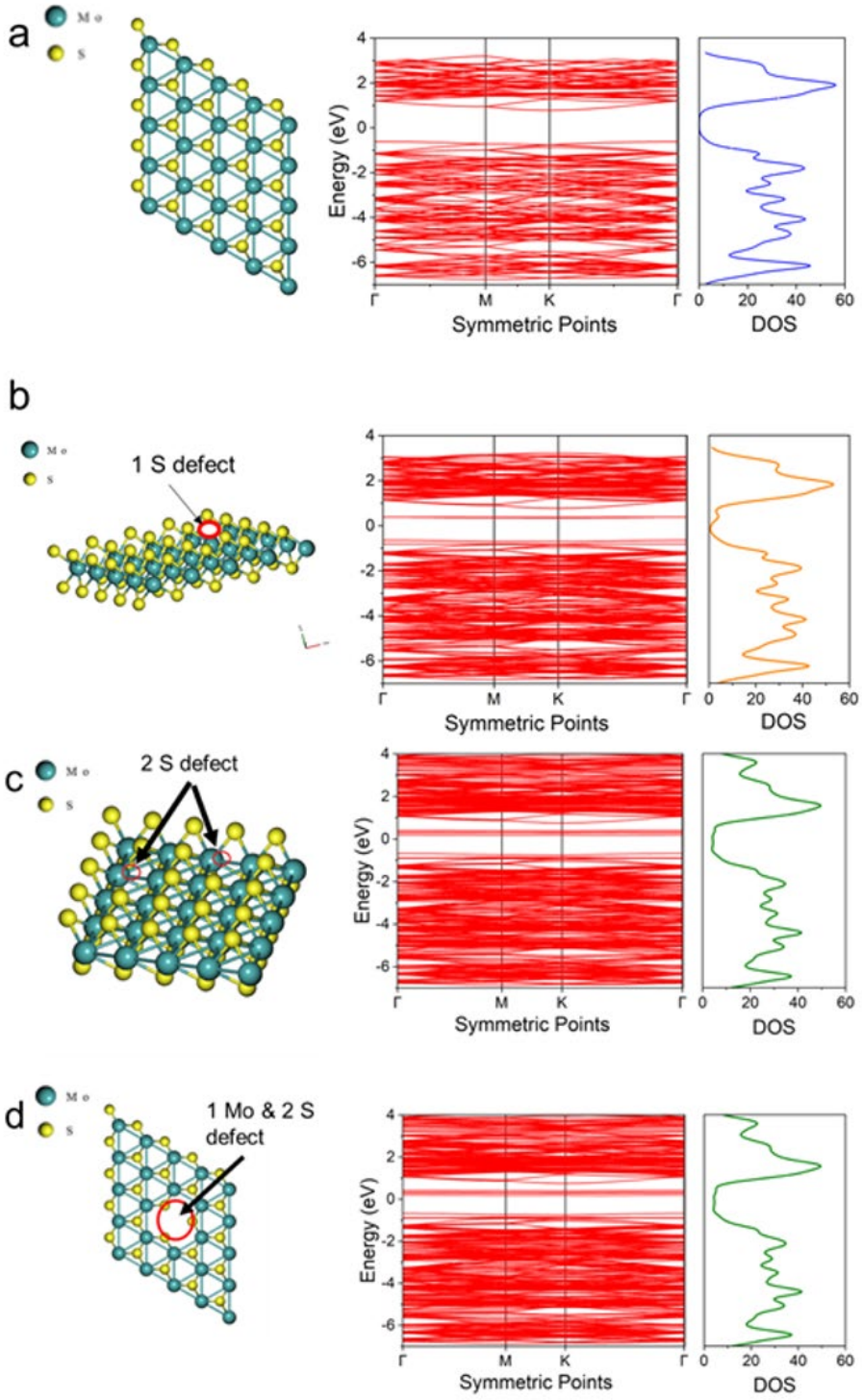

Figure 17. (a) Band structure and density of states of pristine MoS_2. (b) Band structure and density of states of defected MoS_2 with two S defects. (c) Band structure and density of states of defected MoS_2 with one Mo and two S defects. (d) Band structure and density of states of defected MoS_2 with one Mo and two S defects.

5. CONCLUSIONS

The monolayer graphene grown over the metal (Ni, Cu) substrates has very small D peak or there was no D peak in Raman spectrum, which suggests graphene grown by the CVD process is pure in crystalline structure. After the irradiation doses and with the increment of the irradiation doses, the D peak appears and becomes bigger and wider, which is the indication of creation of defects by the gamma irradiation in mono-layer graphene.

Moreover, G peak and 2D peak move right side on Raman spectrum from the previous position, which is called red shift and G peak and 2D peak move left side on Raman spectrum from the previous position, which is called blue shift. There is clear red shift initially and then blue shift occurred in G and 2D peaks in Raman spectra for all samples, which indicates the phonon softening by creating defects in the crystalline structure of the monolayer graphene [17]. The blue shift occurred because of doping in graphene by the charge from the metallic substrate [18].

I_D/I_G curve first increases as irradiation dose increases and then decreases with irradiation dose, further increases for both types of samples (graphene grown over nickel and copper substrates). It indicates that the crystalline structure of the graphene is changing to nanocrystalline and then it changes to the amorphous carbon structure by increasing the irradiation doses [16].

XPS study was performed on exposed and unexposed samples. We can clearly see in that the C-C bond area is decreasing by the increment of irradiation doses for both types of samples. The C-O-C, C-OH and, COOH bond increase with irradiation doses increase, which indicates that the electrical conductivity of graphene decreases with the increase in irradiation doses. As irradiation dose increases, adsorption of oxygen occurs in graphene which leads to degradation in electrical conductivity [19].

In conclusion, we investigated gamma irradiation effects on a monolayer of MoS_2. We studied the changes in the physical properties of MoS_2 using Raman spectroscopy and XPS. The results showed that S defects dominate at lower irradiation, while Mo defects appear at higher irradiation doses. The shifting of Mo 3d and S 2p peaks in the XPS spectra confirmed the presence of S and Mo point defects. DFT studies suggest that, as the gamma irradiation dose increases, the bandgap decreases, which implies that gamma radiation-induced defects degrade the electronic conductivity of MoS_2 monolayer.

REFERENCES

[1] Katsnelson, M.I., 'Graphene: carbon in two dimensions,' *Materials today*, 2007, 10, (1-2), pp. 20-27.
[2] Iqbal, M., Kumar Singh, A., Iqbal, M., Seo, S., and Eom, J., 'Effect of e-beam irradiation on graphene layer grown by chemical vapor deposition,' *Journal of Applied Physics*, 2012, 111, (8), p. 084307.
[3] Neto, A.C., Guinea, F., Peres, N.M., Novoselov, K.S., and Geim, A.K., 'The electronic properties of graphene,' *Reviews of modern physics*, 2009, 81, (1), p. 109.
[4] Sayil, S. and Wang, J., 'Single-event soft errors in CMOS logic,' *IEEE Potentials*, 2012, 31, (2), pp. 15-22.
[5] Zhang, Y., Ma, H.-L., Cao, K., Wang, L., Zeng, X., Zhang, X., He, L., Liu, P., Wang, Z., and Zhai, M., 'Gamma irradiation-induced preparation of graphene–Ni nanocomposites with efficient electromagnetic wave absorption,' *Materials*, 2018, 11, (11), p. 2145.
[6] Lobet, M., Majerus, B., Henrard, L., and Lambin, P., 'Perfect electromagnetic absorption using graphene and epsilon-near-zero metamaterials,' *Physical Review B*, 2016, 93, (23), p. 235424.
[7] Song, W.-L., Cao, M.-S., Lu, M.-M., Bi, S., Wang, C.-Y., Liu, J., Yuan, J., and Fan, L.-Z., 'Flexible graphene/polymer composite films in sandwich structures for effective electromagnetic interference shielding,' *Carbon*, 2014, 66, pp. 67-76.
[8] Ling, J., Zhai, W., Feng, W., Shen, B., Zhang, J., and Zheng, W.G., 'Facile preparation of lightweight microcellular polyetherimide/graphene composite foams for electromagnetic interference shielding,' *ACS applied materials & interfaces*, 2013, 5, (7), pp. 2677-2684.
[9] Liang, J., Wang, Y., Huang, Y., Ma, Y., Liu, Z., Cai, J., Zhang, C., Gao, H., and Chen, Y., 'Electromagnetic interference shielding of graphene/epoxy composites,' *Carbon*, 2009, 47, (3), pp. 922-925.
[10] Hong, S.K., Kim, K.Y., Kim, T.Y., Kim, J.H., Park, S.W., Kim, J.H., and Cho, B.J., 'Electromagnetic interference shielding effectiveness of monolayer graphene,' *Nanotechnology*, 2012, 23, (45), p. 455704.
[11] Shi, S., Chen, F., Ehlerding, E.B., and Cai, W., 'Surface engineering of graphene-based nanomaterials for biomedical applications,' *Bioconjugate chemistry*, 2014, 25, (9), pp. 1609-1619.
[12] Serry, M., Sharaf, A., Emira, A., Abdul-Wahed, A., and Gamal, A., 'Nanostructured graphene–Schottky junction low-bias radiation sensors,' *Sensors and Actuators A, Physical*, 2015, 232, pp. 329-340.
[13] Costa, S.D., Righi, A., Fantini, C., Hao, Y., Magnuson, C., Colombo, L., Ruoff, R.S., and Pimenta, M.A., 'Resonant Raman spectroscopy of graphene grown on copper substrates,' *Solid State Communications*, 2012, 152, (15), pp. 1317-1320.
[14] Compagnini, G., Giannazzo, F., Sonde, S., Raineri, V., and Rimini, E., 'Ion irradiation and defect formation in single layer graphene,' *Carbon*, 2009, 47, (14), pp. 3201-3207.
[15] Boukortt, N., Patanè, S., and Crupi, G., '3D investigation of 8-nm tapered n-FinFET model,' *Silicon*, 2020, 12, (7), pp. 1585-1591.
[16] Mak, K.F., and Shan, J., 'Photonics and optoelectronics of 2D semiconductor transition metal dichalcogenides,' *Nature Photonics*, 2016, 10, (4), pp. 216-226.
[17] Lembke, D., Bertolazzi, S., and Kis, A., 'Single-layer MoS2 electronics,' *Accounts of chemical research*, 2015, 48, (1), pp. 100-110.
[18] Yazyev, O.V., and Kis, A., 'MoS2 and semiconductors in the flatland,' *Materials Today*, 2015, 18, (1), pp. 20-30.
[19] Babu, K., and Goel, E., 'Evolution of Tunnel Field Effect Transistor for Low Power and High Speed Applications: A Review,' *Silicon*, 2022, pp. 1-10.
[20] Nayeri, M., Moradinasab, M., and Fathipour, M., 'The transport and optical sensing properties of MoS2, MoSe2, WS2 and WSe2 semiconducting transition metal dichalcogenides,' *Semiconductor Science and Technology*, 2018, 33, (2), p. 025002.
[21] Ullah, M.S., Yousuf, A.H.B., Es-Sakhi, A.D., and Chowdhury, M.H., 'Analysis of optical and electronic properties of MoS2 for optoelectronics and FET applications,' in Editor (Ed.)^(Eds.), 'Book Analysis of optical and electronic properties of MoS2 for optoelectronics and FET applications' (AIP Publishing LLC, 2018, edn.), p. 020001.
[22] Walker, R., Shi, T., Silva, E., Jovanovic, I., and Robinson, J., 'Radiation effects on two-dimensional materials,' *physica status solidi (a)*, 2016, 213, (12), pp. 3065-3077.
[23] Dudarev, S., 'Density functional theory models for radiation damage,' *Annual Review of Materials Research*, 2013, 43, pp. 35-61.
[24] Łażewski, J., Jochym, P., Piekarz, P., Sternik, M., Parlinski, K., Cholewiński, J., Dłużewski, P., and Krukowski, S., 'DFT modelling of the edge dislocation in 4H-SiC,' *Journal of Materials Science*, 2019, 54, (15), pp. 10737-10745.

REFERENCES (Continued)

[25] Engel, E., and Dreizler, R.M., 'Density functional theory,' *Theoretical and mathematical physics*, 2011, pp. 351-399.
[26] Dobson, J.F., Vignale, G., and Das, M.P., 'Electronic density functional theory: recent progress and new directions,' 2013.
[27] Doyle, B., Arghavani, R., Barlage, D., Datta, S., Doczy, M., Kavalieros, J., Murthy, A., and Chau, R., 'Transistor Elements for 30nm Physical Gate Lengths and Beyond,' *Intel Technology Journal*, 2002, 6, (2).
[28] Ieong, M., Doris, B., Kedzierski, J., Rim, K., and Yang, M., 'Silicon device scaling to the sub-10-nm regime,' *Science*, 2004, 306, (5704), pp. 2057-2060.
[29] Bohr, M.T., and Young, I.A., 'CMOS scaling trends and beyond,' *IEEE Micro*, 2017, 37, (6), pp. 20-29.
[30] Tan, Y., Ma, L., Gao, Z., Chen, M., and Chen, F., 'Two-dimensional heterostructure as a platform for surface-enhanced Raman scattering,' *Nano letters*, 2017, 17, (4), pp. 2621-2626.
[31] Yoon, Y., Ganapathi, K., and Salahuddin, S., 'How good can monolayer MoS2 transistors be?' *Nano letters*, 2011, 11, (9), pp. 3768-3773.
[32] Novoselov, K., Morozov, S., Mohinddin, T., Ponomarenko, L., Elias, D., Yang, R., Barbolina, I., Blake, P., Booth, T., and Jiang, D., 'Electronic properties of graphene,' *physica status solidi (b)*, 2007, 244, (11), pp. 4106-4111.
[33] McCann, E., and Koshino, M., 'The electronic properties of bilayer graphene,' *Reports on Progress in physics*, 2013, 76, (5), p. 056503.
[34] Schwierz, F., 'Graphene transistors,' *Nature nanotechnology*, 2010, 5, (7), pp. 487-496.
[35] Jiang, H., 'Electronic band structures of molybdenum and tungsten dichalcogenides by the GW approach,' *The Journal of Physical Chemistry C*, 2012, 116, (14), pp. 7664-7671.
[36] Ovchinnikov, D., Allain, A., Huang, Y.-S., Dumcenco, D., and Kis, A., 'Electrical transport properties of single-layer WS2,' *ACS nano*, 2014, 8, (8), pp. 8174-8181.
[37] Elías, A.L., Perea-López, N., Castro-Beltrán, A., Berkdemir, A., Lv, R., Feng, S., Long, A.D., Hayashi, T., Kim, Y.A., and Endo, M., 'Controlled synthesis and transfer of large-area WS2 sheets: from single layer to few layers,' *ACS nano*, 2013, 7, (6), pp. 5235-5242.
[38] Ma, Y., Dai, Y., Guo, M., Niu, C., Lu, J., and Huang, B., 'Electronic and magnetic properties of perfect, vacancy-doped, and nonmetal adsorbed MoSe 2, MoTe 2 and WS 2 monolayers,' *Physical Chemistry Chemical Physics*, 2011, 13, (34), pp. 15546-15553.
[39] Di Iorio, Y., Berruet, M., Gau, D., Spera, E., Pereyra, C., Marotti, R., and Vázquez, M., 'Efficiency Improvements in Solution-Based CuInS2 Solar Cells Incorporating a Cl-Doped ZnO Nanopillars Array,' *physica status solidi (a)*, 2017, 214, (12), p. 1700191.
[40] Roldán, R., Silva-Guillén, J.A., López-Sancho, M.P., Guinea, F., Cappelluti, E., and Ordejón, P., 'Electronic properties of single-layer and multilayer transition metal dichalcogenides MX2 (M= Mo, W and X= S, Se),' *Annalen der Physik*, 2014, 526, (9-10), pp. 347-357.
[41] Vogl, T., Sripathy, K., Sharma, A., Reddy, P., Sullivan, J., Machacek, J.R., Zhang, L., Karouta, F., Buchler, B.C., and Doherty, M.W., 'Radiation tolerance of two-dimensional material-based devices for space applications,' *Nature communications*, 2019, 10, (1), pp. 1-10.
[42] Arnold, A.J., Shi, T., Jovanovic, I., and Das, S., 'Extraordinary radiation hardness of atomically thin MoS2,' *ACS applied materials & interfaces*, 2019, 11, (8), pp. 8391-8399.
[43] Chavda, C.P., Srivastava, A., Pradhan, S.K., and Bahoura, M., 'Gamma irradiation effect studies on monolayer CVD grown graphene on metallic substrates,' in Editor (Ed.)^(Eds.), 'Book Gamma irradiation effect studies on monolayer CVD grown graphene on metallic substrates' (International Society for Optics and Photonics, 2020, edn.), p. 113780E.
[44] Chavda, C.P., Veronis, G., Srivastava, A., and Vaughan, E., 'Gamma irradiation effect studies on monolayer molybdenum disulfide on copper substrates,' in Editor (Ed.)^(Eds.), 'Book Gamma irradiation effect studies on monolayer molybdenum disulfide on copper substrates' (International Society for Optics and Photonics, 2021, edn.), p. 115900I.
[45] Li, H., Liu, C., Zhang, Y., Qi, C., Wei, Y., Zhou, J., Wang, T., Ma, G., Tsai, H.-S., and Dong, S., 'Electron radiation effects on the structural and electrical properties of MoS2 field effect transistors,' *Nanotechnology*, 2019, 30, (48), p. 485201.
[46] Foran, B., Mann, C., Peterson, M., Bushmaker, A., Wang, B., Chen, J., Yang, S., and Cronin, S.B., 'Effects of proton radiation-induced defects on optoelectronic properties of MoS 2,' *IEEE Transactions on Nuclear Science*, 2018, 66, (1), pp. 413-419.
[47] Wang, B., Yang, S., Chen, J., Mann, C., Bushmaker, A., and Cronin, S.B., 'Radiation-induced direct bandgap transition in few-layer MoS2,' *Applied Physics Letters*, 2017, 111, (13), p. 131101.

REFERENCES (Continued)

[48] Yockell-Lelièvre, H., Lussier, F., and Masson, J.-F., 'Influence of the particle shape and density of self-assembled gold nanoparticle sensors on LSPR and SERS,' *The Journal of Physical Chemistry C*, 2015, 119, (51), pp. 28577-28585.
[49] Zhao, G.-Y., Deng, H., Tyree, N., Guy, M., Lisfi, A., Peng, Q., Yan, J.-A., Wang, C., and Lan, Y., 'Recent progress on irradiation-induced defect engineering of two-dimensional 2H-MoS2 few layers,' *Applied Sciences*, 2019, 9, (4), p. 678.
[50] Kolhe, P., Thorat, A., Phatangare, A., Jadhav, P., Dalvi, S., Dhole, S., and Dahiwale, S., 'Strain induced study on MoS2 thin films due to ion and gamma irradiation,' *Journal of Alloys and Compounds*, 2022, 896, p. 162969.
[51] Han, S.W., Yun, W.S., Kim, H., Kim, Y., Kim, D.-H., Ahn, C.W., and Ryu, S., 'Hole doping effect of MoS2 via electron capture of He+ ion irradiation,' *Scientific Reports*, 2021, 11, (1), pp. 1-9.
[52] Kim, T.-Y., Cho, K., Park, W., Park, J., Song, Y., Hong, S., Hong, W.-K., and Lee, T., 'Irradiation effects of high-energy proton beams on MoS2 field effect transistors,' *ACS nano*, 2014, 8, (3), pp. 2774-2781.
[53] Durand, C., Zhang, X., Fowlkes, J., Najmaei, S., Lou, J., and Li, A.-P., 'Defect-mediated transport and electronic irradiation effect in individual domains of CVD-grown monolayer MoS2,' *Journal of Vacuum Science & Technology B, Nanotechnology and Microelectronics: Materials, Processing, Measurement, and Phenomena*, 2015, 33, (2), p. 02B110.
[54] Pelella, A., Kharsah, O., Grillo, A., Urban, F., Passacantando, M., Giubileo, F., Iemmo, L., Sleziona, S., Pollmann, E., and Madauß, L., 'Electron irradiation of metal contacts in monolayer MoS2 field-effect transistors,' *ACS Applied Materials & Interfaces*, 2020, 12, (36), pp. 40532-40540.
[55] Zhang, Y., Chen, X., Wang, H., Dai, J., Xue, J., and Guo, X., 'Electronic Properties of Multilayer MoS2 Field Effect Transistor with Unique Irradiation Resistance,' *The Journal of Physical Chemistry C*, 2021, 125, (3), pp. 2089-2096.
[56] Garrity, K.F., Bennett, J.W., Rabe, K.M., and Vanderbilt, D., 'Pseudopotentials for high-throughput DFT calculations,' *Computational Materials Science*, 2014, 81, pp. 446-452.
[57] Giannozzi, P., Baroni, S., Bonini, N., Calandra, M., Car, R., Cavazzoni, C., Ceresoli, D., Chiarotti, G.L., Cococcioni, M., and Dabo, I., 'QUANTUM ESPRESSO: a modular and open-source software project for quantum simulations of materials,' *Journal of physics: Condensed matter*, 2009, 21, (39), p. 395502.
[58] Felix, J.F., Da Silva, A.F., Da Silva, S.W., Qu, F., Qiu, B., Ren, J., De Azevedo, W.M., Henini, M., and Huang, C.-C., 'A comprehensive study on the effects of gamma radiation on the physical properties of a two-dimensional WS 2 monolayer semiconductor,' *Nanoscale Horizons*, 2020, 5, (2), pp. 259-267.
[59] Li, H., Zhang, Q., Yap, C.C.R., Tay, B.K., Edwin, T.H.T., Olivier, A., and Baillargeat, D., 'From bulk to monolayer MoS2: evolution of Raman scattering,' *Advanced Functional Materials*, 2012, 22, (7), pp. 1385-1390.
[60] Bae, S., Sugiyama, N., Matsuo, T., Raebiger, H., Shudo, K.-i., and Ohno, K., 'Defect-induced vibration modes of Ar+-irradiated MoS 2', *Physical Review Applied*, 2017, 7, (2), p. 024001
[61] Parkin, W.M., Balan, A., Liang, L., Das, P.M., Lamparski, M., Naylor, C.H., Rodríguez-Manzo, J.A., Johnson, A.C., Meunier, V., and Drndic, M., 'Raman shifts in electron-irradiated monolayer MoS2,' *ACS nano*, 2016, 10, (4), pp. 4134-4142.
[62] Zhao, H.-Q., Mao, X., Zhou, D., Feng, S., Shi, X., Ma, Y., Wei, X., and Mao, Y., 'Bandgap modulation of MoS 2 monolayer by thermal annealing and quick cooling,' *Nanoscale*, 2016, 8, (45), pp. 18995-19003.
[63] Luo, X., Zhao, Y., Zhang, J., Xiong, Q., and Quek, S.Y., 'Anomalous frequency trends in MoS 2 thin films attributed to surface effects,' *Physical Review B*, 2013, 88, (7), p. 075320.
[64] Castellanos-Gomez, A., Roldán, R., Cappelluti, E., Buscema, M., Guinea, F., van der Zant, H.S., and Steele, G.A., 'Local strain engineering in atomically thin MoS2,' *Nano letters*, 2013, 13, (11), pp. 5361-5366.
[65] Rice, C., Young, R., Zan, R., Bangert, U., Wolverson, D., Georgiou, T., Jalil, R., and Novoselov, K., 'Raman-scattering measurements and first-principles calculations of strain-induced phonon shifts in monolayer MoS 2,' *Physical Review B*, 2013, 87, (8), p. 081307.
[66] Kim, H.J., Kim, D., Jung, S., Bae, M.H., Yun, Y.J., Yi, S.N., Yu, J.S., Kim, J.H., and Ha, D.H., 'Changes in the Raman spectra of monolayer MoS2 upon thermal annealing,' *Journal of Raman Spectroscopy*, 2018, 49, (12), pp. 1938-1944.
[67] Ganta, D., Sinha, S., and Haasch, R.T., '2-D material molybdenum disulfide analyzed by XPS,' *Surface Science Spectra*, 2014, 21, (1), pp. 19-27.
[68] Kondekar, N.P., Boebinger, M.G., Woods, E.V., and McDowell, M.T., 'In situ XPS investigation of transformations at crystallographically oriented MoS2 interfaces,' *ACS applied materials & interfaces*, 2017, 9, (37), pp. 32394-32404.

REFERENCES (Continued)

[69] Lin, G., Zhao, M.-Q., Jia, M., Zhang, J., Cui, P., Wei, L., Zhao, H., Johnson, A.C., Gundlach, L., and Zeng, Y., 'Performance enhancement of monolayer MoS2 transistors by atomic layer deposition of high-k dielectric assisted by Al2O3 seed layer,' *Journal of Physics D: Applied Physics*, 2019, 53, (10), p. 105103.
[70] Zhang, R., Qiao, L., Zhang, H., Zhao, X., Gao, X., and Wang, P., 'Influence of Au2+ ions irradiation on the structure and wear resistance of amorphous MoS2 films,' *Applied Surface Science*, 2022, p. 152497.
[71] Wang, H., Yu, L., Lee, Y.-H., Shi, Y., Hsu, A., Chin, M.L., Li, L.-J., Dubey, M., Kong, J., and Palacios, T., 'Integrated circuits based on bilayer MoS2 transistors,' *Nano letters*, 2012, 12, (9), pp. 4674-4680.
[72] Yun, W.S., Han, S., Hong, S.C., Kim, I.G., and Lee, J., 'Thickness and strain effects on electronic structures of transition metal dichalcogenides: 2H-M X 2 semiconductors (M= Mo, W; X= S, Se, Te),' *Physical Review B*, 2012, 85, (3), p. 033305.

DISTRIBUTION LIST

DTIC/OCP
8725 John J. Kingman Rd, Suite 0944
Ft Belvoir, VA 22060-6218 1 cy

AFRL/RVIL
Kirtland AFB, NM 87117-5776 1 cy

Official Record Copy
AFRL/RVB/Erin I. Vaughan 1 cy